Pis'ma v ZhETF, vol. 102, iss. 5, pp. 316 – 321

Magnetically dependent optical bistability and multistability in an open diamond nitrogen-vacancy centers

R. Karimi, M. Eghbalpour, S. H. Asadpour, S. Batebi[1)], *H. Rahimpour Soleimani*

Department of Physics, University of Guilan, 41335 Rasht, Iran

Submitted 15 July 2015

In this paper we investigate the optical bistability (OB) and optical multistability (OM) behaviors in a unidirectional ring cavity filled with diamond nitrogen-vacancy (NV) defect centers driven by an elliptically polarized probe field in the presence of magnetic field and compare its properties with the corresponding closed system. Our numerical result reveal that threshold of optical bistability and the width of hysteresis loop can be manipulated by adjusting the phase difference between the two circularly polarized components of a single coherent field and cavity parameters, i.e. the electronic exit rate from cavity and electron injection rates. Also it is shown that OB and OM are very sensitive to the relative phase between applied fields and magnetic field. It can be realized that by tuning the parameters the transition from bistability to multistability or vice versa can be obtained.

DOI: 10.7868/S0370274X15170063

1. Introduction. The phenomenon of optical bistability (OB) and optical multibistability (OM) in atomic and semiconductor quantum well (SQW) systems has been the center of interest since late 1980s, due to its potential applications in various fields such as optical transistors, all optical switches and memories [1–9]. In the last decades OB was studied experimentally and theoretically. Some of experimental studies were based on a collection of two-level atomic system interacting with a single mode field [10–13]. Theoretically OB was studied in various atomic and SWQ systems [14–21]. Namely A.J. Feng and his coworkers investigated the effect of control and decay coherence on OB in a SWQ system. They showed that these two mechanisms of quantum coherence can enhance the nonlinear response of SQW structure and consequently the behavior of OB [22]. Chen et al. studied the OB and OM of a three-level atomic system under non-resonant condition [23]. They has shown that only by changing the negative detuning of coupling field into positive detuning the system switches from OB to MB. Under interaction of a strong control field these systems exhibit many interesting outputs, such as electromagnetically induced transparency (EIT) [24–26], optical solitons [27–29], spontaneously generated coherence (SGC) and vacuum induced coherence (VIC) [30, 31]. For example Osman and Joshi studied the OB in a four level system in incoherent pumping interacting with three electromagnetic fields [32]. The system was in an EIT atomic vapor medium. They showed that how one can control the absorption dispersion characteristics of the probe field and OB in an EIT medium with the help of SGC and incoherent pumping. In another study the effect of Doppler broadening on OB in a two-level atomic system was investigated [33].

On the other hand, for solid-state quantum physics experiments and quantum information processing the nitrogen-vacancy (NV) centers in diamond nanocrystal have been appeared as especially strong candidates due to a long electronic spin decoherence time at room temperature, single-shot spin detection, subnanosecond spin control, and efficient quantum state transfer between electron and nearby nuclear spins [34–49]. Zhang et al. [40] investigated laser-polarization dependent and magnetically controlled OB in an optical ring cavity filled with diamond nitrogen-vacancy (NV) defect centers under optical excitation. The phase control absorption-gain and dynamic switching behaviors in a nanodiamond NV center have been theoretically investigated by Li and his coworkers [41]. In our recent study [42], we discuss the group velocity properties of Gaussian beam in a dielectric medium doped with nanodiamond nitrogen vacancy (NV) centers under optical excitation. It is shown that the shape of transmitted and reflected pulses from dielectric can be tuned by changing the intensity of magnetic field and polarization of the control beam.

In this paper we extend the results of previous researchers and investigate the OB and OM behaviors of an open four-level diamond nitrogen-vacancy (NV) defect centers can be adjusted by phase difference between the two circularly polarized components of a single co-

[1)]e-mail: S_Batebi@guilan.ac.ir

herent field and cavity parameters, i.e. the electronic exit rate from cavity and electronic injection rates. An external magnetic field also applies to the system. It is shown that by adjusting the magnetic field one can control the bistable behaviors of the media. In an open model, the levels of system are allowed to exchange population with associated reservoir levels. These levels might, for example, be magnetic sublevels or hyperfine levels. The system is called open because the population that leaves the upper level does not necessarily enter the lower level. In this case the levels are assumed to acquire population at some controllable pump rates.

In the following section, we present the model and density matrix equation of motion. The results are discussed in Sec. 3, and the conclusion can be found in Sec. 4.

2. Model and equations. The medium doped to the slab is nanodiamond NV centers. Nanodiamond NV color centers are consisted of substitutional nitrogen atoms (N) plus a vacancy (V) in an adjacent lattice site as shown in Fig. 1a. The NV center is negatively charged

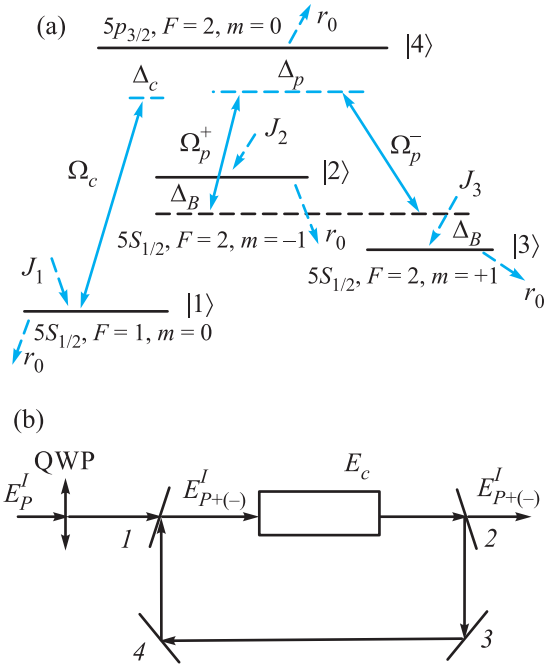

Fig. 1. (a) – Four level diamond NV centers in a tripod-type configuration in the presence of a magnetic field. By applying an external magnetic field, the degeneracy among the ground states $|3\rangle$, $|2\rangle$ is lifted, Δ_B indicates the Zeeman Shift, J_1, J_2, and J_3 are the electronic injection rates for levels $|1\rangle$, $|2\rangle$, and $|3\rangle$, respectively, $r_0 = J_1 + J_2 + J_3$ is the exit rate from the cavity. (b) – Unidirectional ring cavity with a sample of length L, $E^I_{P+(-)}$ and $E^T_{P+(-)}$ are the incident and transmitted fields, respectively, E_c is the coherent control field

with two unpaired electrons located at the vacancy, usually treated as electron spin-1. The spin-spin interaction leads to the energy splitting $D_{gs} = 2.88$ GHz between the ground levels $|^3A, m_s = 0\rangle$ and $|^3A, m_s = \pm 1\rangle$ as depicted in Fig. 1a. By employing an external static magnetic field B along the quantized axis of diamond NV centers, the degeneracy of the ground sublevels $|^3A, m_s = \pm 1\rangle$ can be lifted. We label $|^3A, m_s = 0\rangle$, $|^3A, m_s = -1\rangle$, and $|^3A, m_s = +1\rangle$ as $|1\rangle$, $|2\rangle$, and $|3\rangle$, respectively. The state $|4\rangle$ can be coupled to the ground state $|1\rangle$ with linear polarization [50] and decays to the ground-states sublevels $|2\rangle$ and $|3\rangle$ with radiation of σ^+ and σ^- circular polarization, respectively.

Thus, the transition $|4\rangle \leftrightarrow |1\rangle$ is coupled with a linearly polarized coupling field with a carrier frequency ω_c and one-half Rabi frequency $\Omega_c = \mu_{41}E_c/2\hbar$, where E_c – the amplitude of the coupling is field and μ_{41} is the electric dipole moment for the transition $|4\rangle \leftrightarrow |1\rangle$. A probe field with electric field amplitude E_0 after passing through the quarter-wave plate (QWP) becomes elliptically polarized that has been rotated by an angle θ. An elliptically polarized field can be decomposed into two mutually polarized components as: $E_p = E_p^+\sigma^+ + E_p^-\sigma^-$, where $E_p^+ = E_0/\sqrt{2}(\cos\theta + \sin\theta)e^{i\theta}$ and $E_p^- = E_0/\sqrt{2}(\cos\theta - \sin\theta)e^{-i\theta}$. Here, σ^+ and σ^- are the unit vectors of the right-hand circularly and the left-hand circularly polarized basis, respectively. The strength of the electric field components and phase difference between them can be changed by QWP. Then the Rabi frequency for right-circularly polarized component become $\Omega_{p^+} = \Omega_p(\cos\theta + \sin\theta)e^{i\theta}$ and for left-circularly polarized component is $\Omega_{p^-} = \Omega_p(\cos\theta - \sin\theta)e^{-i\theta}$. Where $\Omega_p = \mu E_0/\sqrt{2}\hbar$, here we assume that $\mu_{42} = \mu_{43} = \mu$. Where J_1, J_2, and J_3 are the electronic injection rates for levels $|1\rangle$, $|2\rangle$, and $|3\rangle$, respectively, r_0 is the exit rate from the cavity. We assumed that the number of interacting electronic is constant, therefore $r_0 = J_1 + J_2 + J_3$.

The equations of motion for the density matrix elements for the electronic meidum under the rotating wave and electric dipole approximations become:

$$\dot{\rho_{44}} = -(\Gamma_{41} + \Gamma_{42} + \gamma_{43})\rho_{44} + i\Omega_c\rho_{14} - i\Omega_c^*\rho_{41} +$$

$$+ i\Omega_p^+\rho_{24} - i\Omega_p^{+*}\rho_{42} + i\Omega_p^-\rho_{34} - i\Omega_p^{-*}\rho_{43} - r_0\rho_{44},$$

$$\dot{\rho_{33}} = -(\Gamma_{32} + \Gamma_{31})\rho_{33} + \Gamma_{43}\rho_{44} - i\Omega_p^-\rho_{34} + i\Omega_p^{+*}\rho_{43} +$$

$$+ r_0\rho_{33} + J_3,$$

$$\dot{\rho_{22}} = \Gamma_{42}\rho_{44} + \Gamma_{32}\rho_{33} - \Gamma_{21}\rho_{22} - i\Omega_p^+\rho_{24} + i\Omega_p^{+*}\rho_{42} -$$

$$- r_0\rho_{22} + J_2,$$

$$\dot{\rho_{11}} = \Gamma_{41}\rho_{44} + \Gamma_{31}\rho_{33} + \Gamma_{21}\rho_{22} - i\Omega_c\rho_{14} + i\Omega_c^*\rho_{41} -$$

$$- r_0\rho_{11} + J_1,$$

$$\dot{\rho}_{14} = -(\gamma_{41}-i\Delta_c)\rho_{14}+i\Omega_c^*(\rho_{44}-\rho_{11})-i\Omega_p^{+*}\rho_{12}-i\Omega_p^{-*}\rho_{13},$$

$$\dot{\rho}_{13} = -\{\gamma_{31}-i[\Delta_c-(\Delta_p+\Delta_B)]\}\rho_{13}+i\Omega_c^*\rho_{43}-i\Omega_p^-\rho_{14},$$

$$\dot{\rho}_{12} = -\{\gamma_{21}-i[\Delta_c-(\Delta_p-\Delta_B)]\}\rho_{12}+i\Omega_c^*\rho_{42}-i\Omega_p^+\rho_{14},$$

$$\dot{\rho}_{23} = -(\gamma_{32}+2i\Delta_B)\rho_{23} + i\Omega_p^{+*}\rho_{43} - i\Omega_p^-\rho_{24},$$

$$\dot{\rho}_{24} = -[\gamma_{42} - i(\Delta_p - \Delta_B)]\rho_{24} + i\Omega_p^{+*}(\rho_{44} - \rho_{22}) - - i\Omega_c^*\rho_{21} - i\Omega_p^{-*}\rho_{23},$$

$$\dot{\rho}_{34} = -[\gamma_{43} - i(\Delta_p + \Delta_B)]\rho_{34} + i\Omega_p^{-*}(\rho_{44} - \rho_{33}) - - i\Omega_c^*\rho_{31} - i\Omega_p^{+*}\rho_{32},$$

$$\rho_{ij} = \rho_{ji}^*. \qquad (1)$$

In the above equations, $\Delta_p = \omega_{43} - \omega_p - \Delta_B = \omega_{42} - - \omega_p + \Delta_B$ and $\Delta_c = \omega_{41} - \omega_c$ are the frequency detuning of the probe and control fields, where ω_{ij} is the frequency deference between levels $|i\rangle$ and $|j\rangle$. The population decay rates and dephasing decay rates are added phenomenologically in the above density matrix equations. The population decay rates from the excited state $|4\rangle$ to the ground state $|j\rangle$ denoted by Γ_{4j} $(j = 1, 2, 3)$ are due primarily to longitudinal optical (LO) phonon emission events at low temperature. The total decay rates γ_{ij} $(i \neq j)$ are given by $\gamma_{41} = \gamma/2 + \gamma_{41}^{dph}$, $\gamma_{42} = \gamma/2 + \gamma_{42}^{dph}$, $\gamma_{43} = \gamma/2 + \gamma_{43}^{dph}$, $\gamma_{31} = \gamma_{31}^{dph}$, $\gamma_{32} = \gamma_{32}^{dph}$, and $\gamma_{21} = \gamma_{21}^{dph}$, where $\gamma = \sum_i \Gamma_{4i}$ and γ_{ij}^{dph} is the dephasing decay rate of the quantum coherence of the $|i\rangle \leftrightarrow |j\rangle$ transitions. If $J_1 = J_2 = J_3 = r_0 = 0$, Eq. (1) changes to that for a closed tripod system.

Now we consider a medium composed of the above described atomic system immersed in unidirectional ring cavity as shown in Fig. 1b. We assume that both mirrors *3* and *4* are perfect reflectors and the intensity reflection and transmission of mirrors *1* and *2* are R and T $(R + T = 1)$ respectively. The dynamic response of the elliptically polarized probe field is governed by Maxwell's equation under slowly varying envelope approximation is

$$\frac{\partial E_p}{\partial t} + c\frac{\partial E_p}{\partial z} = \frac{i\omega_p}{2\varepsilon_0}P(\omega_p), \qquad (2)$$

where $P(\omega_p) = N\mu(\rho_{42} + \rho_{43})$ is the induced polarization. For a perfectly tuned cavity, the boundary conditions in the steady state limit $(\partial/\partial t \to 0)$ are:

$$E_P(L) = \frac{E_P^T}{\sqrt{T}}, \qquad (3a)$$

$$E_P(0) = \sqrt{T}E_P^I + RE_P(L). \qquad (3b)$$

Where L is the length of the atomic sample, E_P^I and E_P^T are the incident and the transmitted field, respectively.

In the mean field limit by using the boundary condition we can describe the steady state behavior of elliptically polarized probe filled by:

$$y = 2x - iC(\rho_{42} + \rho_{43}), \qquad (4)$$

where $y = \frac{\mu E_P^I}{\hbar\sqrt{T}}$ and $x = \frac{\mu E_P^T}{\hbar\sqrt{T}}$ are the normalized input and output fields, respectively, $C = \frac{N\omega_P L\mu^2}{2\hbar\varepsilon_0 cT}$ is cooperation parameter.

In this paper all parameters are scaled by γ, that should be in the order of MHz for diamond NV centers. Following the paper [49], the system parameters are selected as $\gamma = \sum_i \Gamma_{4i} = 2\pi \cdot 13.4\,\text{MHz}$, $\Gamma_{41} = \Gamma_{42} = \Gamma_{43} = \gamma$, and $\Gamma_{32} = 0$, $\gamma_{31} = \Gamma_{21} = 0$.

3. Result and discussion. In this section, we investigate the influence of phase difference between two components of probe field and external magnetic field on optical bistability in closed and open systems. We

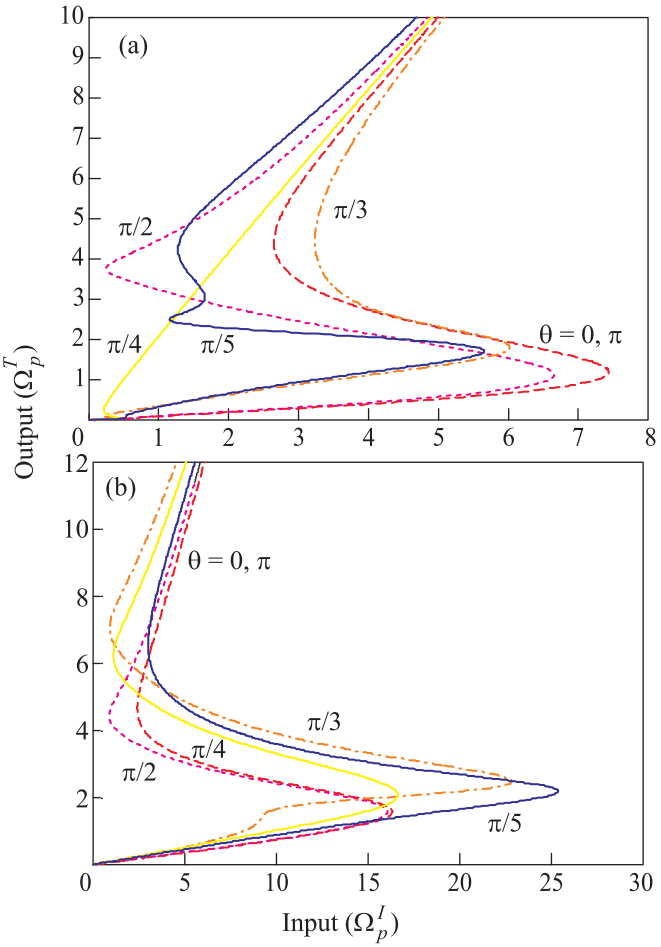

Fig. 2. The output field versus input field for different values of θ for closed, $r_0 = 0$ (a), and open, $r_0 = 1$ (b), systems $j_1 = j_2 = j_3$. The other parameters are $\Delta_B = 1\gamma$, $\Delta_p = 0.5\gamma$, $\Delta_c = -1.5\gamma$, $C = 100$, $\Omega_c = 2\gamma$

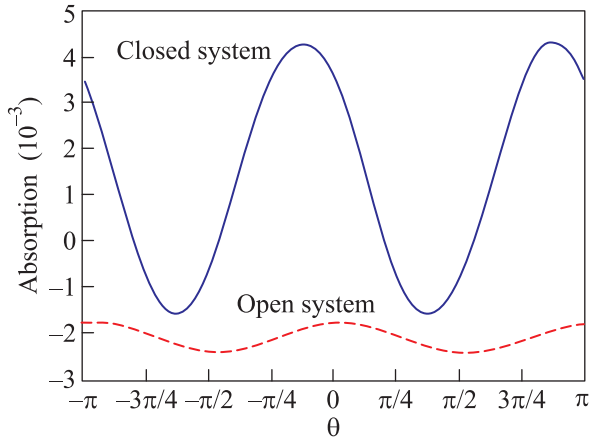

Fig. 3. The absorption of probe field versus phase difference θ for closed (solid line) and open (dashed line) systems. Other parameters are the same as those in Fig. 2

find that the threshold and the width of the bistable region can be manipulated by the relative phase difference (θ) and Zeeman shift ($\Delta_B = 0$). The output field versus input field for different values of θ for closed and open system is depicted in Figs. 2 and 3, with the corresponding values of $\Delta_p = 0.5\gamma$, $\Delta_c = -1.5\gamma$, $C = 100$, $\Omega_c = 2\gamma$ and for open system $r_0 = 1$, $j_1 = j_2 = j_3$. First, we fix the Zeeman shift on $\Delta_b = 1\gamma$ and scanning the influence of the phase difference θ for both systems closed and open. Our numerical results for closed and open systems are shown in Figs. 2a and b respectively. By comparing Figs. 2a and b, it is clear that when the system is open the threshold of bistability increase. We plot the absorption of the probe field versus the phase difference of two components of the probe field in Fig. 3. It can be seen that the absorption of probe field in the open system is less than that in closed system, thus reaching the saturation for open system is harder than closed system so the threshold of bistability increase. When $\theta = \pi/4$, Ω_p^- is zero and the system turns to a typical Λ-type three level system. When phase difference shift to $\theta = \pi/5$ we can observe multi-stability in output-input curve for small range of input field in the closed system. So we can control the threshold value and the hysteresis cycle width of the bistable curve and also we can switch the bistability to multistability and vice versa by adjusting the cavity parameters and phase difference between two components of probe field in the presence of magnetic field.

Next, we fix the phase difference on $\theta = \pi/5$ and analyze the influence of Zeeman shift on bistable behavior of probe field. The numerical result is shown in Fig. 4. When the magnetic field is turned off $\Delta_B = 0$, this system is degenerated as a three-level configura-

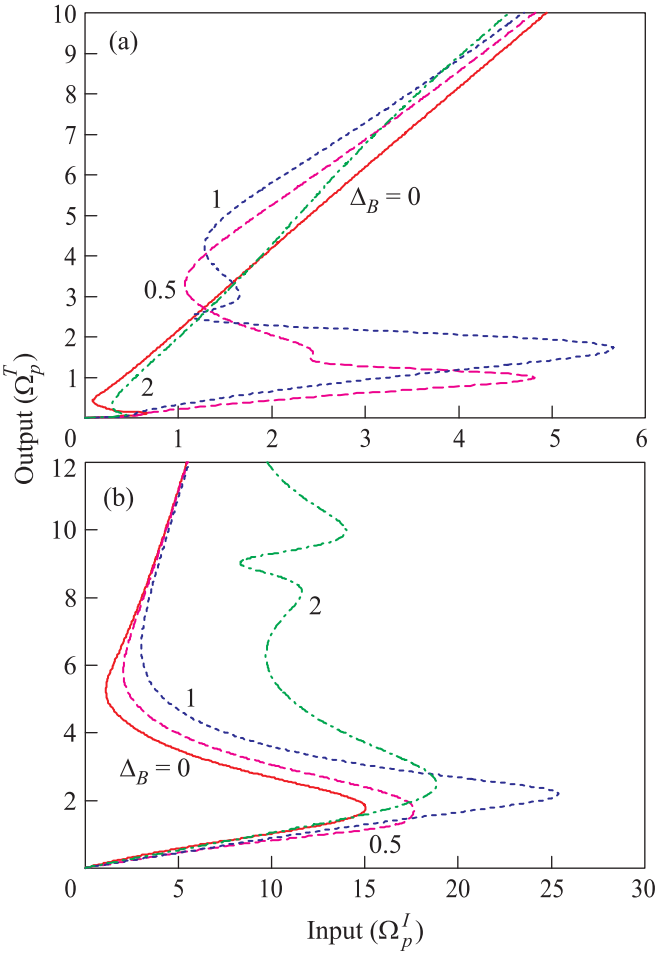

Fig. 4. The output field versus input field for different values of θ for closed, $r_0 = 0$ (a), and open, $r_0 = 1$ (b), systems $j_1 = j_2 = j_3$ when $\theta = \pi/5$. Other parameters are the same as those in Fig. 2

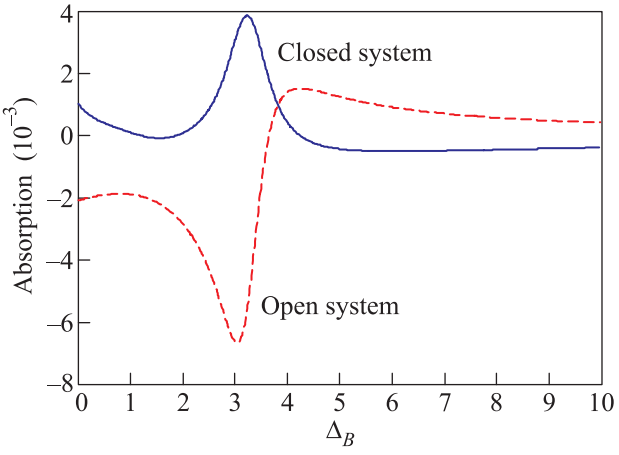

Fig. 5. The absorption of probe field versus Zeeman shift for closed (solid line) and open (dashed line) systems when $\theta = \pi/5$. Other parameters are the same as those in Fig. 2

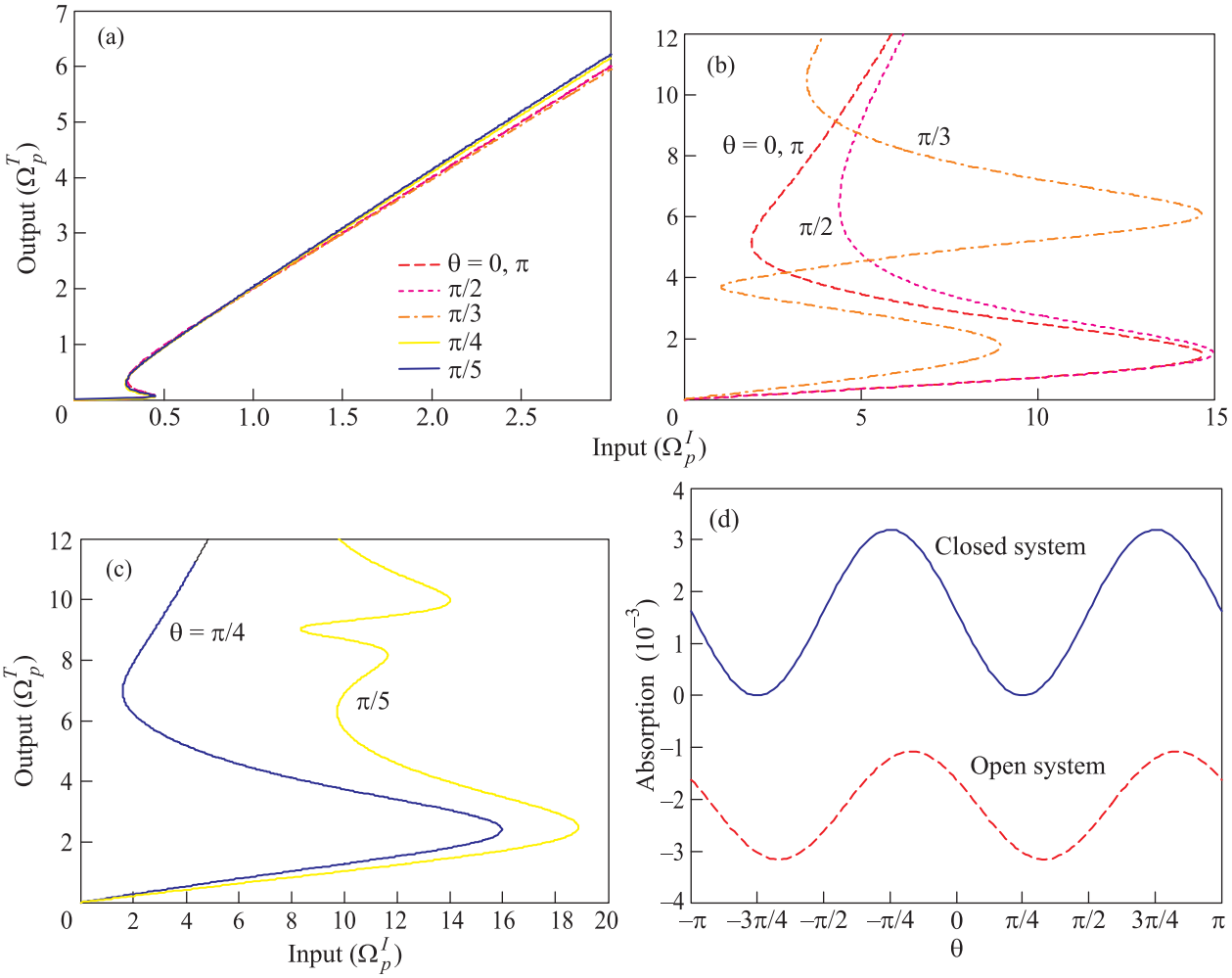

Fig. 6. The output field versus input field for different values of θ for closed, $r_0 = 0$ (a), and open, $r_0 = 1$ (b, c), systems $j_1 = j_2 = j_3$. (d) – The absorption of probe field versus Zeeman shift for closed (solid line) and open (dashed line) systems when $\Delta_B = 2$. Other parameters are the same as those in Fig. 2

tion and after applying the magnetic field the degeneracy of levels lifted. The threshold in the open system is larger than that in closed system because the absorption in open system is less than that in closed system and reaching saturation in open system is harder (see Fig. 5). It is clear from Fig. 4 that in the closed system when $\Delta_B = 1\gamma$ and in open system when $\Delta_B = 2\gamma$ the optical bistability converts to multistability. Note that in the closed system optical multistability occurs for smaller values of input field.

In the following we analyze the effect of phase difference between two components of probe field on input-output behavior of probe field when $\Delta_B = 2\gamma$, other parameters are the same as Fig. 2. By comparing Figs. 2 and 6, we can see that by changing the amount of magnetic field (Δ_B), the behavior of output-input curve varies dramatically. It is essential to note that in this case ($\Delta_B = 2\gamma$) the threshold of the bistability and the width of hysteresis loop in the both systems (open and closed system) decrease. Also it is clear from Fig. 6 that in the open system for some phase difference the bistability curve convert to multistability curve. So, by tuning the relative phase and external magnetic field the transition from bistability to multi-stability or vice versa can be obtained. Also one can manipulate the threshold and width of hysteresis loop with applying appropriate external magnetic field and phase difference between two components of probe field. The absorption of probe field in this case is plotted in Fig. 6d. It is essential to note that when the absorption of probe field is negative, the probe field will be amplified. The amount of gain can be controlled by parameters such as θ, Δ_B and cavity parameters.

3. Conclusion. In conclusion, we propose a scheme for controlling the OB and multistability in a four-level diamond NV centers via external magnetic field, phase

difference between fields and cavity parameters. It is shown that by tuning the relative phase between two components of probe field, the switching between bistability and multistability or vice versa can occur. In this case the relative phase and magnetic field can be used as parameters to control the threshold intensity of the OB and multistability.

1. A. Joshi and M. Xiao, J. Mod. Opt. **57**, 1196 (2010).
2. Z. H. Xiao and K. Kim, Opt. Commun. **283**, 2178 (2010).
3. S. H. Asadpour and A. Eslami-Majd, J. Lumin. **132**, 1477 (2012).
4. W. Harshawerdhen and G. S. Agarwal, Phys. Rev. A **53**, 1812 (1996).
5. M. A. Antón, O. G. Calderón, S. Melle, I. Gonzalo, and F. Carre no, Opt. Commun. **268**, 146 (2006).
6. Z. Wang, A. X. Chen, W. X. Yang, and R. K. Lee, JOSA B **29**, 2891 (2012).
7. J. H. Li, X.Ẏ. Lü, J. M. Luo, and Q. J. Huang, Phys. Rev. A **74**, 035801 (2006).
8. Z. Wang and B. Yu, J. Appl. Phys. **113**, 113101 (2013).
9. L. A. Lugiato, in *Progress in Optics*, ed. by E. Wolf, North-Holland, Amsterdam (1984), v. 21, p. 71.
10. H. J. Gibbs, S. L. McCall, and T. N. C. Venkatesan, Phys. Rev. Lett. **36**, 1135 (1976).
11. A. T. Rosenberger, L. A. Orozco, and H. J. Kimble, Phys. Rev. A **28**, 2569 (1983).
12. L. A. Orozco, H. J. Kimble, A. T. Rosenberger, L. A. Lugiato, M. L. Asquini, M. Brambilla, and L. M. Narducci, ibid. **39**, 1235 (1989).
13. Y. Wu and X. X. Yang, Phys. Rev. A **71**, 053806 (2005).
14. C. Hang and G. Huang, Phys. Rev. A **77**, 033830 (2008).
15. P. Barberis-Blostein, Phys. Rev. A **77**, 013821 (2008).
16. Y. Zhang, A. W. Brown, and M. Xiao, Phys. Rev. Lett. **99**, 123603 (2007).
17. Y. Wu and X. X. Yang, Phys. Rev. A **76**, 013832 (2007).
18. Y. Wu, Phys. Rev. A **71**, 053820 (2005).
19. A. Joshi and M. Xiao, Appl. Phys. B: Lasers Opt. **79**, 65 (2007).
20. J. H. Li, Phys. Rev. B **75**, 155329 (2007).
21. A. J. Feng, C. A. Xi, and D. Li, Chin. Phys. B **22**(2), 024209 (2013).
22. Ch. Ai-Xi, W. Zhi-Ping, Ch. De-Hai, and X. Yan-Qiu, Chinese Phys. B **18**, 1072 (2009).
23. S. E. Harris, J. E. Field, and A. N. Imamoaglu, Phys. Rev. Lett. **64**, 1107 (1990).
24. J. F. Dynes, M. D. Frogley, J. Rodger, and C. C. Phillips, Phys. Rev. B **72**, 085323 (2005).
25. J. P. Marangos, J. Mod. Optics **45**, 471 (1998).
26. Y. F. Zhu, Phys. Rev. A **47**, 495 (1993).
27. W. X. Yang, A. X. Chen, L. G. Si, K. Jiang, X. Yang, and R. K. Lee, Phys. Rev. A **81**, 023814 (2010).
28. W. X. Yang, A. X. Chen, R. K. Lee, and Y. Wu, Phys. Rev. A **84**, 013835 (2011).
29. W. X. Yang, J. M. Hou, and R. K. Lee, Phys. Rev. A **77**, 033838 (2008).
30. X. Lu, J. H. Li, J. B. Liu, and J. M. Luo, J. Phys. B: At. Mol. Opt. Phys. **39**, 5161 (2006).
31. K. I. Osman and A. Joshi, Opt. Comm. **293**, 86 (2013).
32. F. Q. Yuan, L. Y. Jie, and Y. X. Yu, Phys. Rev. A **38**, 4098 (1988).
33. A. T. Rosenberger, L. A. Orozco, and H. J. Kimble, Phys. Rev. A **28**, 2529 (1983).
34. F. Jelezko, T. Gaebel, I. Popa, M. Domhan, A. Gruber, and J. Wrachtrup, Phys. Rev. Lett. **93**, 130 (2004). 51.
35. R. J. Epstein, F. M. Mendoza, Y. K. Kato, and D. D. Awschalom, Nat. Phys. **1**, 94 (2005).
36. T. Gaebel, M. Domhan, I. Popa, C. Wittmann, P. Neumann, F. Jelezko, J. R. Rabeau, N. Stavrias, A. D. Greentree, S. Prawer, J. Meijer, J. Twamley, P. R. Hemmer, and J. Wrachtrup, Nat. Phys. **2**, 8 (2006).
37. M. V. G. Dutt, L. Childress, L. Jiang, E. Togan, J. Maze, F. Jelezko, A. S. Zibrov, P. R. Hemmer, and M. D. Lukin, Science **316**, 1312 (2007).
38. R. Hanson, V. V. Dobrovitski, A. E. Feiguin, O. Gywat, and D. D. Awschalom, Science **320**, 352 (2008).
39. Y. S. Park, A. K. Cook, and H. Wang, Nano Lett. **6**, 2075 (2006).
40. D. Zhang, R. Yu, J. H. Li, C. Ding, and X. Yang, Phys. Lett. A **377**, 2621 (2013).
41. J. H. Li, R. Yu, and X. Yang, Apply. Phys. B **111**, 65 (2013).
42. S. H. Asadpour and H. Rahimpour Soleimani, Physica B. **440**, 124 (2014).
43. M. Larsson, K. N. Dinyari, and H. Wang, Nano Lett. **9**, 1447 (2009).
44. T. van der Sar, Z. H. Wang, M. S. Blok, H. Bernien, T. H. Taminiau, D. M. Toyli, D. A. Lidar, D. D. Awschalom, R. Hanson, and V. V. Dobrovitski, Nature **484**, 82 (2012).
45. G. de Lange, Z. H. Wang, D. Ristè, V. V. Dobrovitski, and R. Hanson, Science **330**, 60 (2010).
46. G. D. Fuchs, A. L. Falk, V. V. Dobrovitski, and D. D. Awschalom, Phys. Rev. Lett. **108**, 157602 (2012).
47. E. Togan, Y. Chu, A. S. Trifonov, L. Jiang, J. Maze, L. Childress, M. V. G. Dutt, A. S. Sørensen, P. R. Hemmer, A. S. Zibrov, and M. D. Lukin, Nature **466**, 730 (2010).
48. W. L. Yang, Z. Q. Yin, Z. Y. Xu, M. Feng, and C. H. Oh, Phys. Rev. A **84**, 043849 (2011).
49. C. Santori, P. E. Barclay, K. M. C. Fu, R. G. Beausoleil, S. Spillane, and M. Fisch, Nanotechnology **21**, 274008 (2010).
50. W. L. Yang, Z. Q. Yin, Z. Y. Xu, M. Feng, and C. H. Oh, Phys. Rev. A **84**, 043849 (2011).